Journal of Thermal Stresses
Publication details, including instructions for authors and subscription information:
http://www.informaworld.com/smpp/title~content=t713723680

Thermo-Mechanical Bending of Functionally Graded Plates

S. Brischetto [a]; R. Leetsch [b]; E. Carrera [a]; T. Wallmersperger [b]; B. Kröplin [b]
[a] Department of Aeronautics and Space Engineering, Politecnico di Torino, Italy
[b] Institute for Statics and Dynamics of Aerospace Structures, Universität Stuttgart, Germany

Online Publication Date: 01 March 2008
To cite this Article: Brischetto, S., Leetsch, R., Carrera, E., Wallmersperger, T. and Kröplin, B. (2008) 'Thermo-Mechanical Bending of Functionally Graded Plates', Journal of Thermal Stresses, 31:3, 286 - 308
To link to this article: DOI: 10.1080/01495730701876775
URL: http://dx.doi.org/10.1080/01495730701876775

Journal of Thermal Stresses, 31: 286–308, 2008
Copyright © Taylor & Francis Group, LLC
ISSN: 0149-5739 print/1521-074X online
DOI: 10.1080/01495730701876775

Taylor & Francis
Taylor & Francis Group

THERMO-MECHANICAL BENDING OF FUNCTIONALLY GRADED PLATES

S. Brischetto[1], R. Leetsch[2], E. Carrera[1], T. Wallmersperger[2], and B. Kröplin[2]

[1]*Department of Aeronautics and Space Engineering, Politecnico di Torino, Italy*

[2]*Institute for Statics and Dynamics of Aerospace Structures, Universität Stuttgart, Germany*

In this work the deformations of a simply supported, functionally graded, rectangular plate subjected to thermo-mechanical loadings are analysed, extending Unified Formulation by Carrera. The governing equations are derived from the Principle of Virtual Displacements accounting for the temperature as an external load only. The required temperature field is not assumed a priori, but determined separately by solving Fourier's equation. Numerical results for temperature, displacement and stress distributions are provided for different volume fractions of the metallic and ceramic constituent as well as for different plate thickness ratios. They correlate very well with three-dimensional solutions given in the literature.

Keywords: Closed form solutions; Functionally graded materials; Mechanical load; Principle of virtual displacements; Refined models; Thermal load; Unified formulation

INTRODUCTION

The severe temperature loads involved in many engineering applications, such as thermal barrier coatings, engine components or rocket nozzles, require high-temperature resistant materials. In Japan in the late 1980s the concept of *Functionally Graded Materials* (FGMs) has been proposed as a thermal barrier material. FGMs are advanced composite materials wherein the composition of each material constituent varies gradually with respect to spatial coordinates. Therefore, in FGMs the macroscopic material properties vary continuously, distinguishing them from laminated composite materials in which the abrupt change of material properties across layer interfaces leads to large interlaminar stresses allowing for damage development. As in the case of laminated composite materials, FGMs combine the desirable properties of the constituent phases to obtain a superior performance, but avoid the problem of interfacial stresses.

Received 11 June 2007; accepted 11 October 2007.

Address correspondence to Salvatore Brischetto, PhD Student, Department of Aeronautics and Space Engineering, Politecnico di Torino, Corso Duca degli Abruzzi, 24, 10129 Torino, Italy. E-mail: salvatore.brischetto@polito.it

In the field of FGMs we face substantially three problems, namely: (1) development of processing routes for functionally graded materials, (2) determination of the spatially varying material properties (material modeling), and (3) modeling of structures comprising FGMs. Even though the attention of the present work is focused on the latter topic, a short discussion including literature overview of the three topics is given.

1. Several techniques have been used for the manufacturing of FGMs, see Burkes and Moore [1], Chung and Das [2], Khor et al. [3] and Kim et al. [4]. For a comprehensive review about the design, processing, modeling as well as applications of FGMs the interested reader is refered to the books by Miyamoto et al. [5] and Suresh and Mortensen [6].

2. Since the determination of macroscopic material properties of inhomogeneous materials in laboratory is very inconvenient for any possible combination of volume fractions of the constituents, a large variety of theoretical models – generally known as micromechanics or homogenization – has been developed. In [7] Aboudi gives an overview of several micromechanical models including simple analytical methods like the Rule of Mixture (ROM) as well as more sophisticated computational models like the Method of Cells (MOC). Pindera et al. [8] indicate that standard micromechanical models reflect the response of FGMs only with restricted validity. This is due to the assumed decoupling of micro- and macroscale by introducing a representative volume element (RVE) that actually cannot be found in FGMs. In [9] Aboudi and co-workers introduce the Higher Order Theory for Functionally Graded Materials (HOTFGM) that explicitly couples micro- and macroscale. Applying HOTFGM, Aboudi et al. [10] analysed the thermo-elastic response of FGMs. Reiter et al. [11] investigated the elastic response of FGMs. They compared results of a finite element discretized microstructure with homogenized models obtained from Mori-Tanaka and self-consistent theory and found good agreement, albeit under certain loading conditions the homogenized models could not reproduce the FGM response correctly. In [12] Zuiker compares several homogenization techniques and specifies simple requirements that micromechanical models should fulfil. Moreover, it is stated that an exponential variation of material properties which is often assumed in FGM structure modeling cannot in general be reproduced by micromechanical models.

3. In the last decade extensive research has been done on modeling of structures comprising FGMs. Cheng and Batra [13] present a three-dimensional analytical solution based on an asymptotic expansion for the thermo-elastic deformation of an elliptic, functionally graded ceramic/metal plate. The through-thickness variation of the volume fraction of the ceramic phase is assumed to be a power law function while the effective material properties are obtained by a Mori-Tanaka approach. In [14] the transient nonlinear thermo-elastic behavior of a functionally graded ceramic/metal plate is investigated by Praveen and Reddy applying the von Karman plate theory and the finite element method. It is found that the response of a plate with material properties between those of ceramics and metals is in general not intermediate to the responses of ceramic and metal plates. Reddy [15] proposes analytical as well as finite element solutions for through-thickness functionally graded plates based on third order shear deformation theory.

The effective material properties are calculated from a simple Rule of Mixture assuming a power law volume fraction distribution of the constituents. The model accounts for thermo-mechanical coupling, time dependency and von Karman-type nonlinearity. In [16] a three-dimensional analytical solution for the thermo-mechanical response of simply supported, functionally graded, rectangular plates is given by Reddy and Cheng using an asymptotic expansion method. Applying Mori–Tanaka's method and assuming a power law volume fraction distribution of the constituents, they investigate the influence of the exponent of the volume fraction law on the structural response under pure thermal or mechanical loads.

In previous authors' work, the Unified Formulation (UF) developed by Carrera for multi-layered structures [17] was extended to account also for functionally graded plates under mechanical loadings. In [18, 19] the Principle of Virtual Displacements (PVD) has been proposed and the extension to Reissner's Mixed Variational Theorem was given in [20]. This work addresses the static response of functionally graded, rectangular plates subjected to thermal loads.

UNIFIED FORMULATION

In case of bi-dimensional multi-layered structures (plates and shells), Unified Formulation (UF) by Carrera [17] permits to obtain a large variety of 2*D* models that differ in the order of used expansion in thickness direction and in the manner the variables are modelled (Equivalent Single Layer (ESL) or Layer Wise (LW) approach). The salient feature of Unified Formulation is the unified manner in which all considered variables and fields (displacement, temperature, material) can be treated. As usual in plate theories, the considered variables and their variation are splitted in a set of thickness functions and the relative terms depending on in-plane coordinates (x, y) only. According to this separation, a general variable $\boldsymbol{a}$ and its respective variation $\delta\boldsymbol{a}$ can be written as:

$$\boldsymbol{a}(x, y, z) = F_\tau(z)\, \boldsymbol{a}_\tau(x, y) \quad \delta\boldsymbol{a}(x, y, z) = F_s(z)\, \delta\boldsymbol{a}_s(x, y) \quad \text{with } \tau, s = 1, \ldots, N \qquad (1)$$

where N is the order of expansion in the thickness direction.

In a multi-layered plate the thickness functions of the considered variables can be assumed for the whole structure (ESL approach) or for each single layer (LW approach). In the former case Taylor polynomials are employed as thickness functions while in the latter combinations of Legendre polynomials are used. For further details about UF for multi-layered structures and the relative assembling procedure we refer the reader to [17], [21], and [22].

Unified Formulation for Displacement Components

Due to the unified treatment of all variables, the three displacement components u_x, u_y and u_z and their relative variations can be modelled via Unified Formulation, irrespective of whether FGM layers or constant property layers (also indicated here as classical layers) are considered. A typical single layer FGM plate is reported in Figure 1, a plate with a FGM interlayer between two different "classical" layers is shown in Figure 2. In case of the ESL model, the expansion of

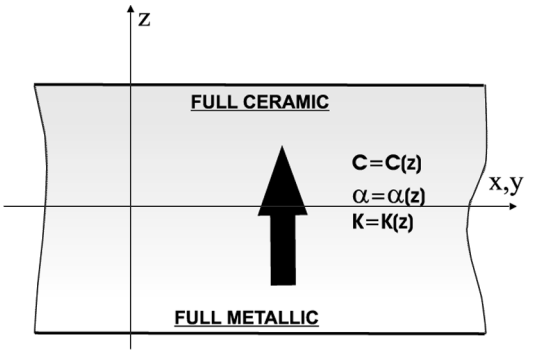

Figure 1 Example of a single-layered FGM plate.

the displacement components is assumed for the whole multi-layer:

$$(u_x, u_y, u_z) = F_\tau(u_{x\tau}, u_{y\tau}, u_{z\tau}) \qquad (\delta u_x, \delta u_y, \delta u_z) = F_s(\delta u_{xs}, \delta u_{ys}, \delta u_{zs}) \tag{2}$$

with Taylor expansions from first up to the 14th-order: $F_0 = z^0 = 1$, $F_1 = z^1 = z, \ldots, F_N = z^N, \ldots, F_{14} = z^{14}$.

The LW model is obtained if we consider separately each layer k of the given multi-layered structure:

$$\left(u_x^k, u_y^k, u_z^k\right) = F_\tau^k\left(u_{x\tau}^k, u_{y\tau}^k, u_{z\tau}^k\right) \qquad \left(\delta u_x^k, \delta u_y^k, \delta u_z^k\right) = F_s^k\left(\delta u_{xs}^k, \delta u_{ys}^k, \delta u_{zs}^k\right) \tag{3}$$

In this case, a combination of Legendre polynomials is employed as thickness functions:

$$F_t = \frac{P_0 + P_1}{2} \quad F_b = \frac{P_0 - P_1}{2} \quad F_l = P_l - P_{l-2} \quad \text{with} \quad \tau, s = t, b, l \text{ and } l = 2, \ldots, 14 \tag{4}$$

Here, t and b indicate the top and bottom values for each layer, P_l are the Legendre polynomials $\left(P_0 = 1, P_1 = \zeta_k, P_2 = \frac{(3\zeta_k^2 - 1)}{2} \text{ and so on}\right)$ with $\zeta_k = \frac{2z^k}{h^k}$ as the non-dimensionalized thickness coordinate ranging from -1 to $+1$ in each layer k. z_k is the local coordinate and h_k the thickness of the kth layer.

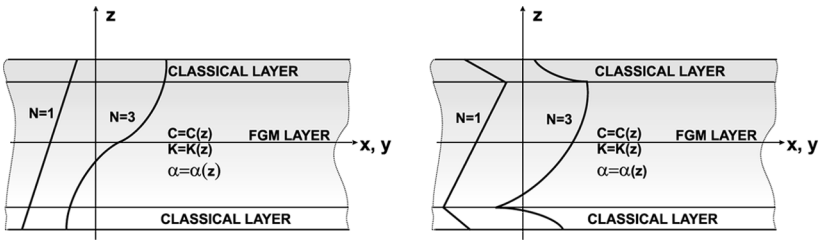

Figure 2 Example of a multi-layered structure with an internal FGM layer: evaluation of the displacement $\boldsymbol{u}$ in case of Equivalent Single-Layer model (left) and Layer-Wise model (right).

The chosen functions have the following interesting properties:

$$\begin{cases} \zeta_k = +1: & F_t = 1; & F_b = 0; & F_l = 0 & \text{at the top} \\ \zeta_k = -1: & F_t = 0; & F_b = 1; & F_l = 0 & \text{at the bottom} \end{cases} \tag{5}$$

Typical ESL and LW displacement evaluations through the thickness direction of a multi-layered FGM plate are reported in Figure 2. It is obvious from Figures 1 and 2 that for a single layer plate the ESL and LW evaluations coincide.

Unified Formulation for Temperature Profile

In the present model the temperature is seen as an external loading. If the values of the temperature are known at the top and bottom surface of the plate, the thermal load can be considered in two different ways. The first method introduces an assumed profile $T(z)$ that varies linearly from the top to the bottom; the second one computes $T(z)$ by solving Fourier's heat conduction equation. In this article only the second way is considered. Even for a very thin FGM layer the temperature profile is nonlinear. Therefore, the assumption of a linear $T(z)$ would cause very large errors.

The temperature profile is described in the same way as the displacements in case of the Layer-Wise approach:

$$T^k(x, y, z) = F_\tau \theta^k_\tau \qquad \text{with} \quad \tau = t, b, l \text{ and } l = 2, \ldots, 14 \tag{6}$$

Again, t and b indicate top and bottom of the considered kth layer. The thickness functions F_τ are a combination of Legendre polynomials.

If the temperature was assumed linear through the thickness, the two values at the top and bottom surface, and therefore F_t and F_b, would be sufficient to describe the assumed profile via UF. The calculation procedure for the actual temperature in case of FGM layers is reported in Appendix A, giving the values of θ^k_τ for Eq. (6).

Application of the Unified Formulation to the Elastic and Thermal Properties of FGMs

In FGM layers the elastic and thermal properties change continuously in thickness direction. The variation of the elastic characteristics is usually given in terms of exponential and/or polynomial functions applied directly to the engineering constants such as Young's Moduli E_i, Shear Moduli G_{ij}, Bulk Moduli B_i and/or Poisson ratio v_{ij} or directly to the material stiffnesses C_{ij}. Actually, since in each point of the plate a relation between the engineering constants and the material stiffnesses holds, only the second case can be treated. Generally, the variation of the stiffness matrix in the thickness direction can be described by multiplying a material constant by a function of z, i.e.,

$$\boldsymbol{C}(z) = \boldsymbol{C}_0 \cdot f(z) \tag{7}$$

The same variation in the thickness direction can be supposed for the thermal conductivity coefficients K_i and the thermal expansion coefficients α_i:

$$\boldsymbol{K}(z) = \boldsymbol{K}_0 \cdot g(z) \tag{8}$$

$$\boldsymbol{\alpha}(z) = \boldsymbol{\alpha}_0 \cdot h(z) \tag{9}$$

The thermo-mechanical coupling coefficients are given by:

$$\boldsymbol{\lambda}(z) = \boldsymbol{C}(z) \cdot \boldsymbol{\alpha}(z) = \boldsymbol{C}_0 \cdot \boldsymbol{\alpha}_0 \cdot m(z) \tag{10}$$

The procedure does not depend on the thickness laws $f(z)$, $g(z)$, $h(z)$, and $m(z)$. Thus, any possible material gradient can be accounted for. Now, applying the ideas behind UF, the following expansions are made:

$$\boldsymbol{C}(z) = F_b(z)\boldsymbol{C}_b + F_\gamma(z)\boldsymbol{C}_\gamma + F_t(z)\boldsymbol{C}_t = F_r\boldsymbol{C}_r \tag{11}$$

$$\boldsymbol{K}(z) = F_b(z)\boldsymbol{K}_b + F_\gamma(z)\boldsymbol{K}_\gamma + F_t(z)\boldsymbol{K}_t = F_r\boldsymbol{K}_r \tag{12}$$

$$\boldsymbol{\alpha}(z) = F_b(z)\boldsymbol{\alpha}_b + F_\gamma(z)\boldsymbol{\alpha}_\gamma + F_t(z)\boldsymbol{\alpha}_t = F_r\boldsymbol{\alpha}_r \tag{13}$$

$$\boldsymbol{\lambda}(z) = F_b(z)\boldsymbol{\lambda}_b + F_\gamma(z)\boldsymbol{\lambda}_\gamma + F_t(z)\boldsymbol{\lambda}_t = F_r\boldsymbol{\lambda}_r \tag{14}$$

where the thickness functions F_r are taken in the same manner as in the LW expansion:

$$F_t = \frac{P_0 + P_1}{2} \quad F_b = \frac{P_0 - P_1}{2} \quad F_\gamma = P_\gamma - P_{\gamma-2} \quad \text{with } \gamma = 2, \ldots, N_r \tag{15}$$

Figure 3 explains the above expansion procedure in case of the stiffness matrix, the same loop is employed for all material properties.

The actual values of $\boldsymbol{C}$, $\boldsymbol{K}$, $\boldsymbol{\alpha}$, and $\boldsymbol{\lambda}$ are then recovered as a weighted summation on the terms $\boldsymbol{C}_r$, $\boldsymbol{K}_r$, $\boldsymbol{\alpha}_r$, and $\boldsymbol{\lambda}_r$, respectively. The weights are given by the thickness functions F_r. The order of the expansion can be freely chosen as for the displacements. In this article the maximum value of N_r is 10. It is mandatory to choose such a high order of expansion to ensure the necessary accuracies.

The procedure to include the varying stiffnesses, thermal conductivity, thermal expansion and coupling coefficients in the model requires the computation of the $\boldsymbol{C}_r$, $\boldsymbol{K}_r$, $\boldsymbol{\alpha}_r$, and $\boldsymbol{\lambda}_r$ arrays. This task can be accomplished by solving for each component C_{ijr}, K_{ir}, α_{ir}, and λ_{ir} a simple algebraic system of order N_r. The actual values are calculated at N_r different locations along the thickness $(z_1, \ldots, z_{N_r})$.

$$\begin{bmatrix} (C_{ij}, K_i, \alpha_i, \lambda_i)(z_1) \\ \vdots \\ (C_{ij}, K_i, \alpha_i, \lambda_i)(z_{N_r}) \end{bmatrix} = \begin{bmatrix} F_b(z_1) & \cdots & F_\gamma(z_1) & \cdots & F_t(z_1) \\ \vdots & & \vdots & & \vdots \\ F_b(z_{N_r}) & \cdots & F_\gamma(z_{N_r}) & \cdots & F_t(z_{N_r}) \end{bmatrix} \begin{bmatrix} C_{ijb}, K_{ib}, \alpha_{ib}, \lambda_{ib} \\ \vdots \\ C_{ijr}, K_{ir}, \alpha_{ir}, \lambda_{ir} \\ \vdots \\ C_{ijt}, K_{it}, \alpha_{it}, \lambda_{it} \end{bmatrix} \tag{16}$$

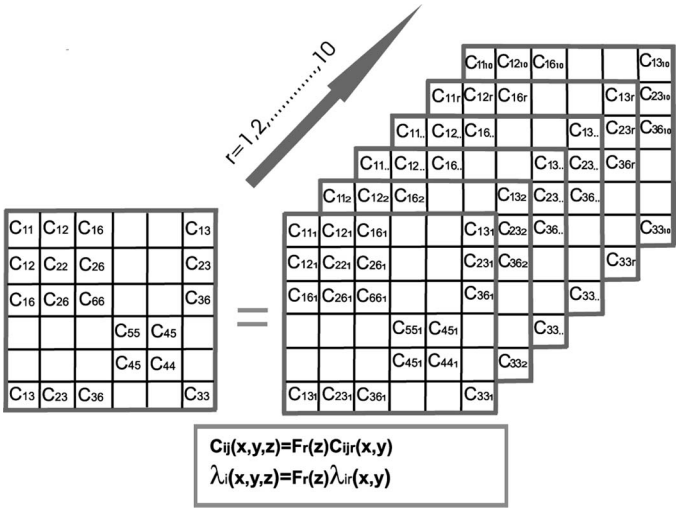

Figure 3 Example of the assembling procedure for the elastic coefficients array in case of a FGM layer.

GOVERNING EQUATIONS

This section presents the derivation of the governing equations based on the *Principle of Virtual Displacements* (PVD) in the case of a FGM plate subjected to thermal and/or external mechanical loads. A closed form solution will be developed considering particular material and boundary conditions. The procedure permits to obtain the so-called *fundamental nuclei*, which are simple matrices representing the basic element from which the stiffness matrices of the whole structure can be computed.

We consider a multi-layered plate with N_l layers, some of which could be FGM layers. The PVD for the thermo-mechanical case reads:

$$\sum_{k=1}^{N_l} \int_{\Omega_k} \int_{A_k} \left\{ \delta \boldsymbol{\epsilon}_{pG}^{k^T} \boldsymbol{\sigma}_{pC}^k + \delta \boldsymbol{\epsilon}_{nG}^{k^T} \boldsymbol{\sigma}_{nC}^k \right\} d\Omega_k dz = \sum_{k=1}^{N_l} \delta L_e^k \tag{17}$$

where Ω_k and A_k are the integration domains in plane (x, y) and z direction, respectively. k indicates the layer and T the transpose of a vector. δL_e^k is the external work for the kth layer. G means geometrical relations and C constitutive ones. $\boldsymbol{\sigma}_{pC}$ and $\boldsymbol{\sigma}_{nC}$ contain the mechanical (d) and thermal (t) contributions, so:

$$\sum_{k=1}^{N_l} \int_{\Omega_k} \int_{A_k} \left\{ \delta \boldsymbol{\epsilon}_{pG}^{k^T} \left(\boldsymbol{\sigma}_{pd}^k - \boldsymbol{\sigma}_{pt}^k \right) + \delta \boldsymbol{\epsilon}_{nG}^{k^T} \left(\boldsymbol{\sigma}_{nd}^k - \boldsymbol{\sigma}_{nt}^k \right) \right\} d\Omega_k dz = \sum_{k=1}^{N_l} \delta L_e^k \tag{18}$$

The steps to obtain the governing equations are:

- Substitution of geometrical relations (subscript G)
- Substitution of appropriate constitutive equations (subscript C)
- Introduction of the Unified Formulation.

Geometrical Relations

From this point on, stresses and strains are going to be separated into in-plane and normal components denoted respectively by the subscripts p and n. Mechanical strains in the kth layer can be related to the displacement field $\boldsymbol{u}^k = \{u_x^k, u_y^k, u_z^k\}$ via the geometrical relations:

$$\boldsymbol{\epsilon}_p^k = \boldsymbol{D}_p \boldsymbol{u}^k \quad \boldsymbol{\epsilon}_n^k = (\boldsymbol{D}_{np} + \boldsymbol{D}_{nz}) \boldsymbol{u}^k \tag{19}$$

wherein the differential operator arrays are defined as follows

$$\boldsymbol{D}_p = \begin{bmatrix} \partial_x & 0 & 0 \\ 0 & \partial_y & 0 \\ \partial_y & \partial_x & 0 \end{bmatrix} \quad \boldsymbol{D}_{np} = \begin{bmatrix} 0 & 0 & \partial_x \\ 0 & 0 & \partial_y \\ 0 & 0 & 0 \end{bmatrix} \quad \boldsymbol{D}_{nz} = \begin{bmatrix} \partial_z & 0 & 0 \\ 0 & \partial_z & 0 \\ 0 & 0 & \partial_z \end{bmatrix} \tag{20}$$

with $\boldsymbol{\epsilon}_p = (\epsilon_1, \epsilon_2, \epsilon_6) = (\epsilon_{xx}, \epsilon_{yy}, \epsilon_{xy})$ and $\boldsymbol{\epsilon}_n = (\epsilon_5, \epsilon_4, \epsilon_3) = (\epsilon_{xz}, \epsilon_{yz}, \epsilon_{zz})$. Here, $\boldsymbol{\epsilon}_p$ and $\boldsymbol{\epsilon}_n$ contain both mechanical and thermal contributions.

Constitutive Equations

In case of thermo-mechanical problems, the constitutive equations are given as:

$$\begin{aligned} \boldsymbol{\sigma}_{pC}^k &= \boldsymbol{\sigma}_{pd}^k - \boldsymbol{\sigma}_{pt}^k = \boldsymbol{C}_{pp}^k(z)\, \boldsymbol{\epsilon}_{pG}^k + \boldsymbol{C}_{pn}^k(z)\, \boldsymbol{\epsilon}_{nG}^k - \boldsymbol{\lambda}_p^k(z) T^k \\ \boldsymbol{\sigma}_{nC}^k &= \boldsymbol{\sigma}_{nd}^k - \boldsymbol{\sigma}_{nt}^k = \boldsymbol{C}_{np}^k(z)\, \boldsymbol{\epsilon}_{pG}^k + \boldsymbol{C}_{nn}^k(z)\, \boldsymbol{\epsilon}_{nG}^k - \boldsymbol{\lambda}_n^k(z) T^k \end{aligned} \tag{21}$$

where the coefficients $\boldsymbol{\lambda}_p^k(z)$ and $\boldsymbol{\lambda}_n^k(z)$ are linked to the coefficients of thermal expansion $\boldsymbol{\alpha}_p^k(z)$ and $\boldsymbol{\alpha}_n^k(z)$ by:

$$\begin{aligned} \boldsymbol{\lambda}_p^k(z) &= \boldsymbol{\lambda}_{pp}^k(z) + \boldsymbol{\lambda}_{pn}^k(z) = \boldsymbol{C}_{pp}^k(z)\, \boldsymbol{\alpha}_p^k(z) + \boldsymbol{C}_{pn}^k(z)\, \boldsymbol{\alpha}_n^k(z) \\ \boldsymbol{\lambda}_n^k(z) &= \boldsymbol{\lambda}_{np}^k(z) + \boldsymbol{\lambda}_{nn}^k(z) = \boldsymbol{C}_{np}^k(z)\, \boldsymbol{\alpha}_p^k(z) + \boldsymbol{C}_{nn}^k(z)\, \boldsymbol{\alpha}_n^k(z) \end{aligned} \tag{22}$$

with

$$\begin{aligned} \boldsymbol{C}_{pp}^k(z) &= \begin{bmatrix} C_{11}(z) & C_{12}(z) & C_{16}(z) \\ C_{12}(z) & C_{22}(z) & C_{26}(z) \\ C_{16}(z) & C_{26}(z) & C_{66}(z) \end{bmatrix} \quad \boldsymbol{C}_{pn}^k(z) = \begin{bmatrix} 0 & 0 & C_{13}(z) \\ 0 & 0 & C_{23}(z) \\ 0 & 0 & C_{36}(z) \end{bmatrix} \\ \boldsymbol{C}_{np}^k(z) &= \begin{bmatrix} 0 & 0 & 0 \\ 0 & 0 & 0 \\ C_{13}(z) & C_{23}(z) & C_{36}(z) \end{bmatrix} \quad \boldsymbol{C}_{nn}^k(z) = \begin{bmatrix} C_{55}(z) & C_{45}(z) & 0 \\ C_{45}(z) & C_{44}(z) & 0 \\ 0 & 0 & C_{33}(z) \end{bmatrix} \end{aligned} \tag{23}$$

The thermal expansion coefficients and the coefficients of thermo-mechanical coupling are:

$$\boldsymbol{\alpha}_p^k(z) = \begin{bmatrix} \alpha_1(z) \\ \alpha_2(z) \\ \alpha_6(z) \end{bmatrix} \quad \boldsymbol{\alpha}_n^k(z) = \begin{bmatrix} 0 \\ 0 \\ \alpha_3(z) \end{bmatrix} \quad \boldsymbol{\lambda}_p^k(z) = \begin{bmatrix} \lambda_1(z) \\ \lambda_2(z) \\ \lambda_6(z) \end{bmatrix} \quad \boldsymbol{\lambda}_n^k(z) = \begin{bmatrix} 0 \\ 0 \\ \lambda_3(z) \end{bmatrix} \tag{24}$$

Applying the extension of UF to FGM plates, the material coefficients are modelled in the following way:

$$\left(\boldsymbol{C}^k_{pp}(z), \boldsymbol{C}^k_{pn}(z), \boldsymbol{C}^k_{np}(z), \boldsymbol{C}^k_{nn}(z)\right) = F_r(z)\left(\boldsymbol{C}^k_{ppr}, \boldsymbol{C}^k_{pnr}, \boldsymbol{C}^k_{npr}, \boldsymbol{C}^k_{nnr}\right) \tag{25}$$

$$\left(\boldsymbol{\lambda}^k_{p}(z), \boldsymbol{\lambda}^k_{n}(z)\right) = F_r(z)\left(\boldsymbol{\lambda}^k_{pr}, \boldsymbol{\lambda}^k_{nr}\right) \tag{26}$$

with $r = 1, \ldots, 10$.

Therefore, in case of FGM plates, the constitutive equations Eqs. (21) read:

$$\begin{aligned} \boldsymbol{\sigma}^k_{pC} &= \boldsymbol{\sigma}^k_{pd} - \boldsymbol{\sigma}^k_{pt} = F_r \boldsymbol{C}^k_{ppr} \boldsymbol{\epsilon}^k_{pG} + F_r \boldsymbol{C}^k_{pnr} \boldsymbol{\epsilon}^k_{nG} - F_r \boldsymbol{\lambda}^k_{pr} T^k \\ \boldsymbol{\sigma}^k_{nC} &= \boldsymbol{\sigma}^k_{nd} - \boldsymbol{\sigma}^k_{nt} = F_r \boldsymbol{C}^k_{npr} \boldsymbol{\epsilon}^k_{pG} + F_r \boldsymbol{C}^k_{nnr} \boldsymbol{\epsilon}^k_{nG} - F_r \boldsymbol{\lambda}^k_{nr} T^k \end{aligned} \tag{27}$$

Differential Equilibrium Equations

Substituting the geometrical relations Eqs. (19) and constitutive equations Eqs. (27) into the variational statement Eq. (17), we obtain for the kth layer:

$$\begin{aligned} \int_{\Omega_k} \int_{A_k} \Big[&\left(\boldsymbol{D}_p \delta \boldsymbol{u}^k\right)^T \left(F_r \boldsymbol{C}^k_{ppr} \boldsymbol{D}_p \boldsymbol{u}^k + F_r \boldsymbol{C}^k_{pnr} \left(\boldsymbol{D}_{np} + \boldsymbol{D}_{nz}\right) \boldsymbol{u}^k - F_r \boldsymbol{\lambda}^k_{pr} T^k\right) \\ &+ \left(\left(\boldsymbol{D}_{np} + \boldsymbol{D}_{nz}\right) \delta \boldsymbol{u}^k\right)^T \left(F_r \boldsymbol{C}^k_{npr} \boldsymbol{D}_p \boldsymbol{u}^k + F_r \boldsymbol{C}^k_{nnr} \left(\boldsymbol{D}_{np} + \boldsymbol{D}_{nz}\right) \boldsymbol{u}^k \right. \\ &\left. - F_r \boldsymbol{\lambda}^k_{nr} T^k\right) \Big] d\Omega_k dz = \delta L^k_e \end{aligned} \tag{28}$$

Now, we implement the expansions of UF Eqs. (2), (3) and (6), yielding:

$$\begin{aligned} \int_{\Omega_k} \int_{A_k} \Big[&\left(\boldsymbol{D}_p F_s \delta \boldsymbol{u}^k_s\right)^T \left(F_r \boldsymbol{C}^k_{ppr} \boldsymbol{D}_p F_\tau \boldsymbol{u}^k_\tau + F_r \boldsymbol{C}^k_{pnr} \left(\boldsymbol{D}_{np} + \boldsymbol{D}_{nz}\right) F_\tau \boldsymbol{u}^k_\tau - F_r \boldsymbol{\lambda}^k_{pr} F_\tau \theta^k_\tau\right) \\ &+ \left(\left(\boldsymbol{D}_{np} + \boldsymbol{D}_{nz}\right) F_s \delta \boldsymbol{u}^k_s\right)^T \left(F_r \boldsymbol{C}^k_{npr} \boldsymbol{D}_p F_\tau \boldsymbol{u}^k_\tau \right. \\ &\left. + F_r \boldsymbol{C}^k_{nnr} \left(\boldsymbol{D}_{np} + \boldsymbol{D}_{nz}\right) F_\tau \boldsymbol{u}^k_\tau - F_r \boldsymbol{\lambda}^k_{nr} F_\tau \theta^k_\tau\right) \Big] d\Omega_k dz = \delta L^k_e \end{aligned} \tag{29}$$

Introducing the following notations:

$$\left(E_{\tau sr}, E_{\tau_{,z} sr}, E_{\tau s_{,z} r}, E_{\tau_{,z} s_{,z} r}\right) = \int_{A_k} \left(F_\tau F_s F_r, F_{\tau_{,z}} F_s F_r, F_\tau F_{s_{,z}} F_r, F_{\tau_{,z}} F_{s_{,z}} F_r\right) dz \tag{30}$$

where, z indicates the partial derivative with respect to z, Eq. (29) can be written in compact form as:

$$\begin{aligned} \int_{\Omega_k} \Big[&\left(\boldsymbol{D}_p \delta \boldsymbol{u}^k_s\right)^T \left(E_{\tau sr} \boldsymbol{C}^k_{ppr} \boldsymbol{D}_p \boldsymbol{u}^k_\tau + E_{\tau sr} \boldsymbol{C}^k_{pnr} \boldsymbol{D}_{np} \boldsymbol{u}^k_\tau + E_{\tau_{,z} sr} \boldsymbol{C}^k_{pnr} \boldsymbol{u}^k_\tau - E_{\tau sr} \boldsymbol{\lambda}^k_{pr} \theta^k_\tau\right) \\ &+ \left(\boldsymbol{D}_{np} \delta \boldsymbol{u}^k_s\right)^T \left(E_{\tau sr} \boldsymbol{C}^k_{npr} \boldsymbol{D}_p \boldsymbol{u}^k_\tau + E_{\tau sr} \boldsymbol{C}^k_{nnr} \boldsymbol{D}_{np} \boldsymbol{u}^k_\tau + E_{\tau_{,z} sr} \boldsymbol{C}^k_{nnr} \boldsymbol{u}^k_\tau - E_{\tau sr} \boldsymbol{\lambda}^k_{nr} \theta^k_\tau\right) \\ &+ \left(\delta \boldsymbol{u}^k_s\right)^T \left(E_{\tau s_{,z} r} \boldsymbol{C}^k_{npr} \boldsymbol{D}_p \boldsymbol{u}^k_\tau + E_{\tau s_{,z} r} \boldsymbol{C}^k_{nnr} \boldsymbol{D}_{np} \boldsymbol{u}^k_\tau + E_{\tau_{,z} s_{,z} r} \boldsymbol{C}^k_{nnr} \boldsymbol{u}^k_\tau - E_{\tau sr} \boldsymbol{\lambda}^k_{nr} \theta^k_\tau\right) \Big] d\Omega_k \\ &= \delta L^k_e \end{aligned} \tag{31}$$

After integration by parts, the governing differential equations on domain Ω_k and boundary conditions on edge Γ_k are obtained. Further details on the procedure of integration by parts are reported in [19].

The governing equations for a FGM multi-layered plate subjected to thermal and mechanical loadings are:

$$\delta \boldsymbol{u}_s^{k\,T} : \boldsymbol{K}_{uu}^{k\tau sr} \boldsymbol{u}_\tau^k = \boldsymbol{K}_{u\theta}^{k\tau sr} \boldsymbol{\theta}_\tau^k + \boldsymbol{P}_{u\tau}^k \tag{32}$$

where $(\boldsymbol{K}_{u\theta}^{k\tau sr} \boldsymbol{\theta}_\tau^k)$ is the thermal load and $\boldsymbol{P}_{u\tau}^k$ is the external mechanical one. The fundamental nuclei $\boldsymbol{K}_{uu}^{k\tau sr}$ and $\boldsymbol{K}_{u\theta}^{k\tau sr}$ have to be assembled by expanding the indices as described in the following: in case of a FGM layer, an internal loop on index r accounts for the variation of the material properties, via τ and s we consider the expansion in z for the considered variables, and via k the assembling on the number of layers is accomplished.

The fundamental nuclei are:

$$\begin{aligned}
\boldsymbol{K}_{uu}^{k\tau sr} = & -\boldsymbol{D}_p^T \left(E_{\tau sr} \boldsymbol{C}_{ppr}^k \boldsymbol{D}_p + E_{\tau sr} \boldsymbol{C}_{pnr}^k \boldsymbol{D}_{np} + E_{\tau_{,z} sr} \boldsymbol{C}_{pnr}^k \right) \\
& - \boldsymbol{D}_{np}^T \left(E_{\tau sr} \boldsymbol{C}_{npr}^k \boldsymbol{D}_p + E_{\tau sr} \boldsymbol{C}_{nnr}^k \boldsymbol{D}_{np} + E_{\tau_{,z} sr} \boldsymbol{C}_{nnr}^k \right) \\
& + E_{\tau s_{,z} r} \boldsymbol{C}_{npr}^k \boldsymbol{D}_p + E_{\tau s_{,z} r} \boldsymbol{C}_{nnr}^k \boldsymbol{D}_{np} + E_{\tau_{,z} s_{,z} r} \boldsymbol{C}_{nnr}^k
\end{aligned} \tag{33}$$

$$\boldsymbol{K}_{u\theta}^{k\tau sr} = -\boldsymbol{D}_p^T \left(-E_{\tau sr} \boldsymbol{\lambda}_{pr}^k \right) - \boldsymbol{D}_{np}^T \left(-E_{\tau sr} \boldsymbol{\lambda}_{nr}^k \right) - E_{\tau sr} \boldsymbol{\lambda}_{nr}^k \tag{34}$$

Closed Form Solutions

A Navier-type closed form solution is obtained via substitution of harmonic expressions for the displacements and temperature as well as considering transversely isotropic materials.

The following harmonic assumptions can be made for the field variables:

$$\begin{aligned}
u_{x_\tau}^k &= \sum_{m,n} \left(\widehat{U}_{x_\tau}^k \right) \cos\left(\frac{m\pi x_k}{a_k} \right) \sin\left(\frac{n\pi y_k}{b_k} \right) \quad k = 1, N_l \\
u_{y_\tau}^k &= \sum_{m,n} \left(\widehat{U}_{y_\tau}^k \right) \sin\left(\frac{m\pi x_k}{a_k} \right) \cos\left(\frac{n\pi y_k}{b_k} \right) \quad \tau = t, b, r \\
u_{z_\tau}^k &= \sum_{m,n} \left(\widehat{U}_{z_\tau}^k \right) \sin\left(\frac{m\pi x_k}{a_k} \right) \sin\left(\frac{n\pi y_k}{b_k} \right) \quad r = 2, N \\
\theta_\tau^k &= \sum_{m,n} \left(\hat{\theta}_\tau^k \right) \sin\left(\frac{m\pi x_k}{a_k} \right) \sin\left(\frac{n\pi y_k}{b_k} \right)
\end{aligned} \tag{35}$$

where $\widehat{U}_{x_\tau}^k$, $\widehat{U}_{y_\tau}^k$, $\widehat{U}_{z_\tau}^k$, and $\hat{\theta}_\tau^k$ are the amplitudes, m and n the wave numbers, and a_k and b_k the plate dimensions.

The explicit forms of the fundamental nuclei $\boldsymbol{K}_{uu}^{k\tau sr}$ and $\boldsymbol{K}_{u\theta}^{k\tau sr}$ are given in Appendix B. If $\theta_\tau^k = 0$ in Eq. (32), only a mechanical load is considered. Vice versa, if $\boldsymbol{P}_{u\tau}^k = 0$, only a thermal load is applied. If we consider a multi-layered structure comprising FGM and/or "classical" layers, two types of assembling procedures are

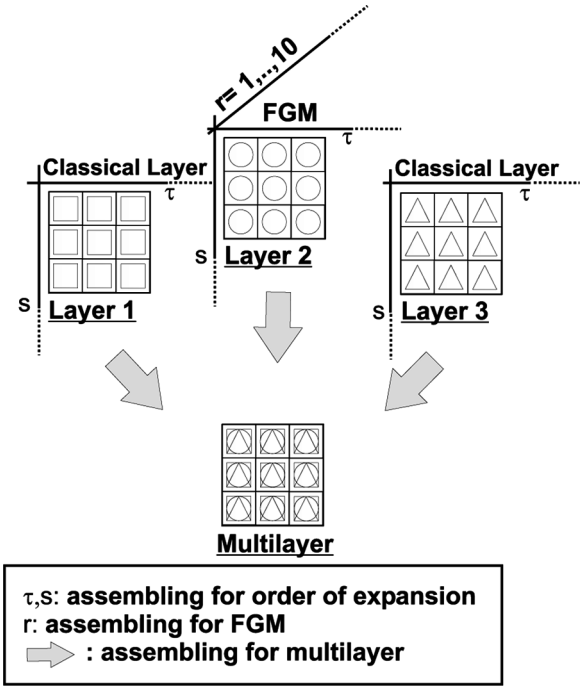

Figure 4 Example of assembling procedure for nucleus $\boldsymbol{K}^{k\tau sr}$ in case of a multi-layered plate with an internal FGM layer: ESL model.

possible: Equivalent Single Layer approach as indicated in Figure 4 and Layer Wise model as illustrated in Figure 5. The fundamental nuclei are formally the same in case of "classical" or FGM layers. The only difference is the assembling loop on index r which accounts for the variation of material properties through the thickness. In case of a single FGM layer, no multi-layer assembling procedure is necessary. Thus, in this case there is no difference between ESL or LW modeling.

Implemented Theories

The proposed assessment considers only one FGM layer, with two different loading conditions: a pure mechanical or thermal load, both applied at the top of the plate. In the case of only one layer, there is no difference between ESL or LW models. So, the proposed kinematics are indicated with the order N used for the description of the displacement $\boldsymbol{u}$ and the temperature T along the thickness direction ($N = 1, \ldots, 14$) where the same order is used for these two variables. The proposed model is able to describe multi-layered FGM/classical structures also. These new benchmarks will be proposed in a future authors' work.

RESULTS AND DISCUSSION

To validate the theory presented in the previous sections, we consider a plate problem for which a three-dimensional solution was given in [16]. A rectangular

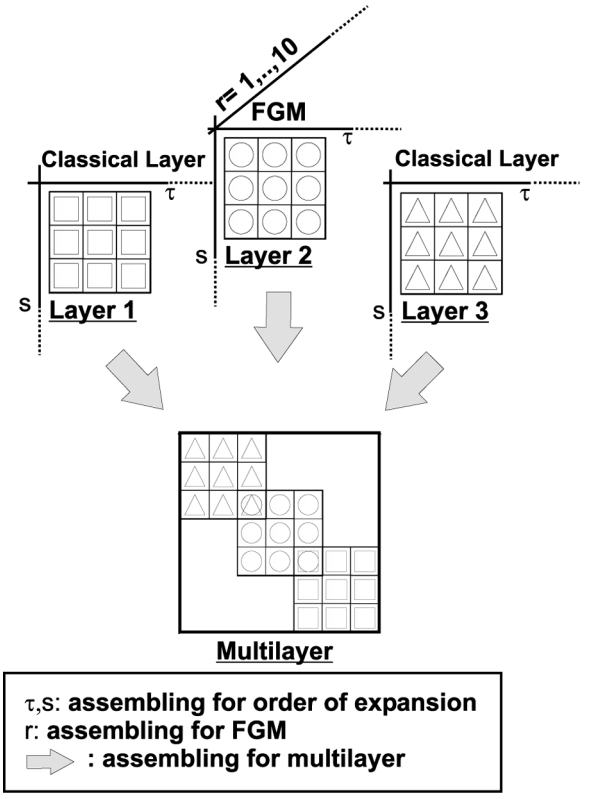

Figure 5 Example of assembling procedure for nucleus $\boldsymbol{K}^{k\tau sr}$ in case of a multi-layered plate with an internal FGM layer: LW model.

plate comprising a single functionally graded layer, as shown in Figure 6, is analyzed. As a typical example for high-temperature applications, the constituent materials of the functionally graded plate are taken to be Monel (70Ni-30Cu), a nickel-based alloy, and the ceramic zirconia (ZrO_2). The required material properties are those reported in [16]:

$$B_m = 227.24\,\text{GPa}, \quad \mu_m = 65.55\,\text{GPa},$$

$$\alpha_m = 15 \times 10^{-6}/\text{K}, \quad K_m = 25\,\text{W/mK}, \quad \text{for Monel}$$

$$B_c = 125.83\,\text{GPa}, \quad \mu_c = 58.08\,\text{GPa},$$

$$\alpha_c = 10 \times 10^{-6}/\text{K}, \quad K_c = 2.09\,\text{W/mK}, \quad \text{for zirconia}$$

For this two-phase composite material different micromechanical models can be applied for the computation of the effective local material properties. According

$$p_z^+(x,y) = \hat{p}_z^+ \sin\left(\frac{m\pi}{a}x\right)\sin\left(\frac{n\pi}{b}y\right)$$

or

$$T_z^+(x,y) = \hat{T}_z^+ \sin\left(\frac{m\pi}{a}x\right)\sin\left(\frac{n\pi}{b}y\right)$$

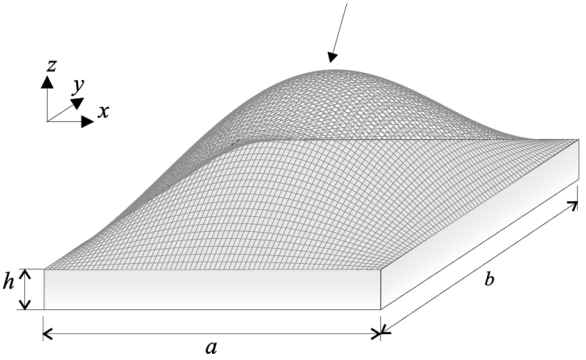

Figure 6 Considered plate for the numerical assessment: a single-layered, functionally graded plate subjected to pure thermal or pure mechnanical bi-sinusoidal loads.

to [16], we choose the following formulas:

- The effective bulk modulus B and shear modulus μ are given by the mean field estimate of Mori and Tanaka [23, 24]:

$$\frac{B - B_m}{B_c - B_m} = \frac{V_2}{1 + (1 - V_2)\frac{B_c - B_m}{B_m + \frac{4}{3}\mu_m}} \tag{36}$$

$$\frac{\mu - \mu_m}{\mu_c - \mu_m} = \frac{V_2}{1 + (1 - V_2)\frac{\mu_c - \mu_m}{\mu_m + f_1}} \quad \text{with } f_1 = \frac{\mu_m(9B_m + 8\mu_m)}{6(B_m + 2\mu_m)} \tag{37}$$

- The effective heat conduction coefficient K is given by the model of Hatta and Taya [25]:

$$\frac{K - K_m}{K_c - K_m} = \frac{V_2}{1 + (1 - V_2)\frac{K_c - K_m}{3K_m}} \tag{38}$$

- For the coefficient of thermal expansion α a correspondence relation holds [26, 27], reading:

$$\frac{\alpha - \alpha_m}{\alpha_c - \alpha_m} = \frac{\frac{1}{B} - \frac{1}{B_m}}{\frac{1}{B_c} - \frac{1}{B_m}} \tag{39}$$

In Eqs. (36) to (39), the indices m and c refer to the metallic and ceramic phase, respectively. V_2 is the volume fraction of the ceramic phase that is assumed for the computations as

$$V_2 = V_c = (z/h)^{n_g} \tag{40}$$

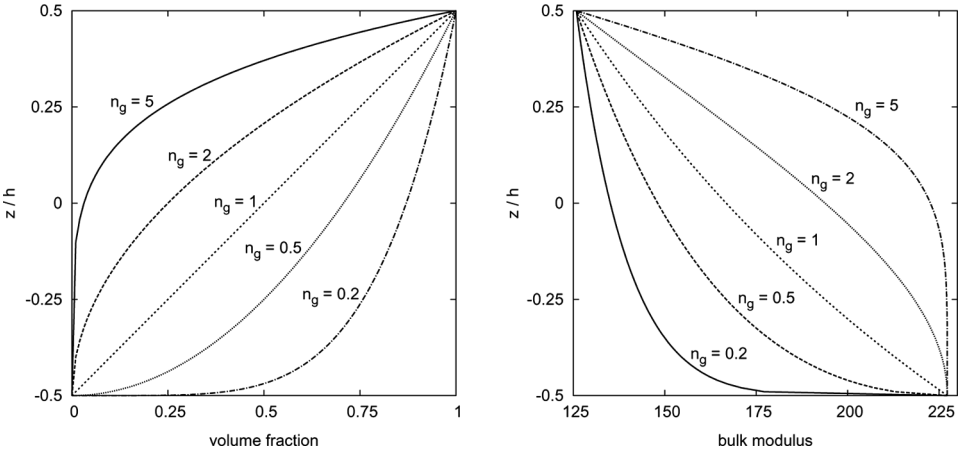

Figure 7 Through-thickness distribution of the volume fraction V_c of the ceramic phase (left) and of the bulk modulus (right).

where by changing the exponent n_g different material gradients can be accomplished. Figure 7 shows the through-thickness distribution of the volume fraction V_c of the ceramic phase and the resulting evolution of the bulk modulus.

At the top surface the plate is subjected to pure mechanical or pure thermal, transverse bi-sinusoidal loads, see Figure 6, reading:

$$p_z^+ = \hat{p}_z^+ \sin\left(\frac{m\pi x}{a}\right)\sin\left(\frac{n\pi y}{b}\right) \quad T^+ = \widehat{T}^+ \sin\left(\frac{m\pi x}{a}\right)\sin\left(\frac{n\pi y}{b}\right) \tag{41}$$

Here m, n are the wave numbers and a, b the plate dimensions, respectively. A quantity with a superimposed hat denotes the amplitude of the respective load. Since we propose a linear theory, more complicated load cases can be accomplished by superimposing the pure thermal and mechanical contributions.

As we consider an analytical Navier-type solution, the plate is assumed to be simply supported, i.e. the boundary conditions read

$$\begin{aligned} u_y = u_z = 0 \quad &\text{at } x = 0, a \\ u_x = u_z = 0 \quad &\text{at } y = 0, b \\ T = 0 \quad &\text{at } x = 0, a \text{ and } y = 0, b \end{aligned} \tag{42}$$

which is fulfilled by the assumed harmonic in-plane displacement and temperature fields, compare Eqs. (35). In addition, we assume $m = n = 1$ for the wave numbers.

As done in [16], non-dimensionalized quantities are introduced:

$$\bar{u}_i = \frac{\hat{u}_i(z)}{Pa} \qquad \bar{\sigma}_{ij} = \frac{\hat{\sigma}_{ij}(z)}{PB^*} \qquad \overline{T} = \frac{\alpha^* \widehat{T}(z)}{P} \tag{43}$$

where either $P = \hat{p}_z^+ / B^*$ or $P = \alpha^* \widehat{T}^+$ is taken for the applied load p_z^+ or for the applied temperature T^+ at the top, respectively. The scale factors are $B^* = 1\,\text{GPa}$ and $\alpha^* = 1 \times 10^6$. The indices i and j can be x, y, and z.

Analysis of the Temperature Profile T(z)

Since in the present model the temperature is taken into account as an external loading only, its through-thickness distribution must be given a priori as an input to the formulation. In the literature the temperature field is often assumed to vary linearly between the plate's top and bottom surface, see e.g., [28]. To compute the actual through-thickness distribution of the temperature for any given material gradient n_g and plate dimensions, the theory reported in Appendix A has been used in this work. The boundary conditions at the top and bottom surface of the plate read, respectively,

$$\overline{T}^+ = 1 \quad \text{at } z = +\frac{h}{2} \qquad \overline{T}^- = 0 \quad \text{at } z = -\frac{h}{2} \tag{44}$$

Figure 8 depicts the through-thickness distribution of the non-dimensionalized temperature $\overline{T}$ for a plate thickness ratio of $a/h = 10$, $a/b = 1$ and different material gradients n_g. For comparison reasons the temperature variation for a "classical" layer with constant material properties is also shown. It can be clearly seen that the temperature distribution of a functionally graded layer differs significantly from that of a "classical" layer. Furthermore, it is obvious that the temperature distribution is strongly nonlinear which contradicts the assumption of a linear temperature variation often found in the literature. Even for the "classical" layer it is seen that the consideration of the three-dimensional Fourier equation, see Eq. (48) in

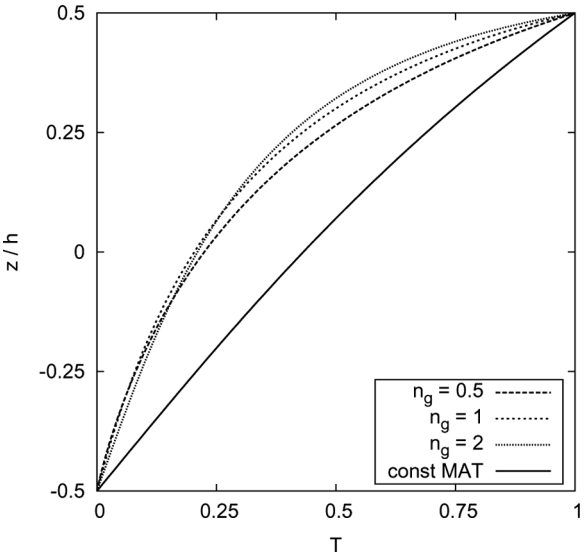

Figure 8 Through-thickness distribution of the non-dimensionalized temperature $\overline{T}$.

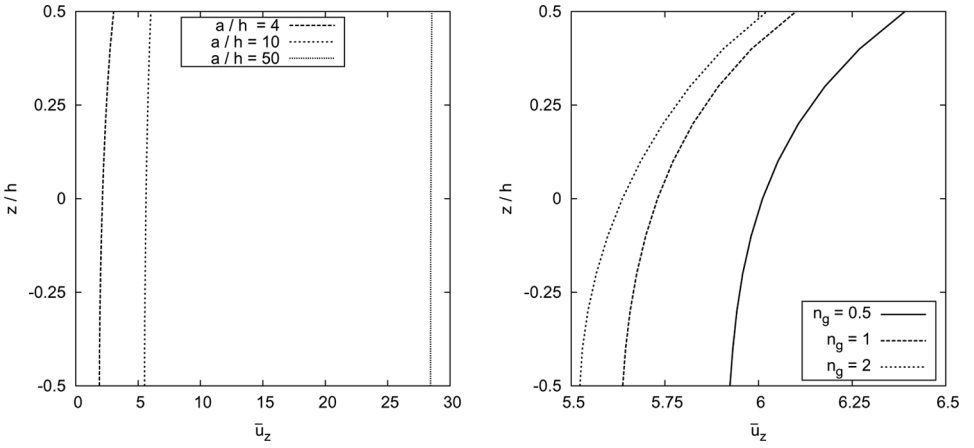

Figure 9 Through-thickness distribution of the non-dimensionalized transverse deflection $\bar{u}_z$ due to a thermal load for different plate thickness ratios ($n_g = 2$) (left) and for different material gradients ($a/h = 10$) (right).

Appendix A, leads to a nonlinear temperature distribution if the layer is subjected to a non-constant thermal load. Concerning the alteration of the temperature distribution due to different material gradients n_g the influence of the material composition is considerable.

Transverse Deflection under Thermal or Mechanical Load

In Figures 9 and 10 the through-thickness distribution of the transverse deflection u_z is shown for different plate thickness ratios ($a/h = 4, 10, 50$) and material gradients ($n_g = 0.5, 1, 2$), respectively, taking $a/b = 1$. It can be clearly seen

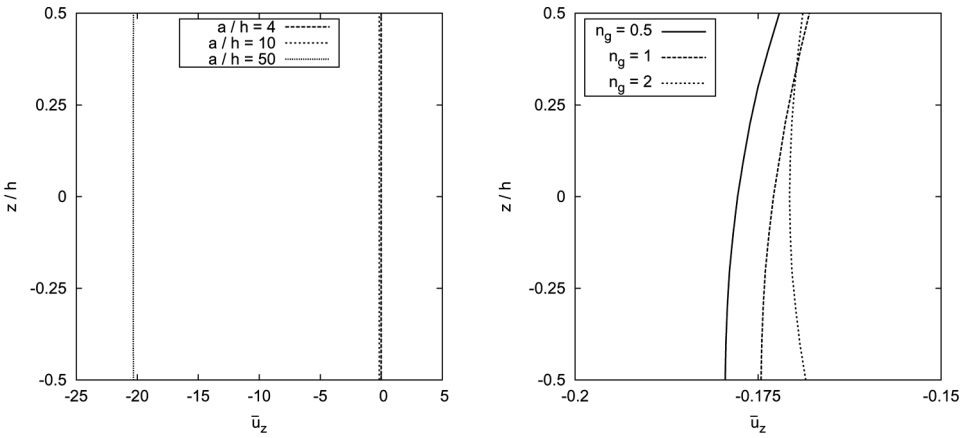

Figure 10 Through-thickness distribution of the non-dimensionalized transverse deflection $\bar{u}_z$ due to a mechanical load for different plate thickness ratios ($n_g = 2$) (left) and for different material gradients ($a/h = 10$) (right).

Table 1 Mechanical load; Non-dimensional transverse displacement $\bar{u}_z$ and in-plane displacement $\bar{u}_x$ at top (t), middle (m) and bottom (b) of the considered plate ($n_g = 2$)

	$a/h = 4$				$a/h = 10$			
	3*D*	$N = 1$	$N = 3$	$N = 5$	3*D*	$N = 1$	$N = 3$	$N = 5$
$\bar{u}_z$(t)	−13.46	−11.23	−13.46	−13.46	−168.9	−126.2	−168.9	−168.9
$\bar{u}_z$(m)	−13.70	−10.83	−13.71	−13.70	−170.7	−125.9	−170.7	−170.7
$\bar{u}_z$(b)	−12.73	−10.43	−12.73	−12.73	−168.5	−125.5	−168.5	−168.5
$\bar{u}_x$(t)	4.021	2.932	4.020	4.022	26.17	19.29	26.17	26.17
$\bar{u}_x$(m)	−0.08998	−0.05419	−0.09095	−0.08991	0.7108	0.7807	0.7109	0.7112
$\bar{u}_x$(b)	−4.069	−3.041	−4.067	−4.069	−24.72	−17.73	−24.72	−24.72

3*D* solution is reported in [16].

from Figure 9 that in the case of a thermal loading the transverse deflection varies considerably through the thickness. Therefore, the usual assumption of a constant through-thickness distribution of u_z made by most lower-order plate theories is not justified in the thermal case. As it is seen from Figure 9, the influence of different material gradients n_g is substantial for a thermal loading. This is due to the combined effects of the varying thermal field – and therefore the loading – as well as the altering mechanical properties. However, in the case of a pure mechanical loading, the influence of different material gradients n_g is less pronounced, see Figure 10. Furthermore, as can be seen from this figure, the variation of the transverse deflection u_z through the thickness is small. Therefore, in the mechanical case the assumption of a constant through-thickness distribution is valid.

The results obtained by UF for a pure thermal or pure mechanical loading are compared with three-dimensional solutions reported by Reddy and Cheng in [16]. Tables 1–4 provide results for the in-plane stress (σ_{xx}) and transverse shear/normal stresses (σ_{xz}) and (σ_{zz}) in non-dimensionalized form for different plate thickness ratios, taking $a/b = 1$ and the exponential index $n_g = 2$. It can be concluded that Unified Formulation yields very accurate results compared to 3*D* solutions both for the mechanical and the thermal case and even for very thick plates. However, to capture all effects of the displacement and stress distributions higher-order plate theories are necessary. Comparing the cases of thermal and mechanical loading,

Table 2 Mechanical load; Non-dimensional stresses $\bar{\sigma}_{ij}$ at top (t), middle (m) and bottom (b) of the considered plate ($n_g = 2$)

	$a/h = 4$				$a/h = 10$			
	3*D*	$N = 2$	$N = 4$	$N = 5$	3*D*	$N = 2$	$N = 4$	$N = 5$
$\bar{\sigma}_{xx}$(t)	−3.154	−2.8473	−3.152	−3.154	−18.17	−16.96	−18.17	−18.17
$\bar{\sigma}_{xx}$(m)	−0.2037	−0.3079	−0.2027	−0.2038	−0.8722	−1.498	−0.8738	−0.8726
$\bar{\sigma}_{xx}$(b)	3.631	3.633	3.633	3.632	22.06	22.88	22.06	22.06
$\bar{\sigma}_{xz}$(m)	−0.9500	−0.6854	−0.9535	−0.9500	−2.396	−1.739	−2.398	−2.396
$\bar{\sigma}_{zz}$(m)	−0.5130	−0.7165	−0.5110	−0.5131	−0.5142	−1.691	−0.5166	−0.5143

3*D* solution is reported in [16].

Table 3 Thermal load; Non-dimensional transverse displacement $\bar{u}_z$ and in-plane displacement $\bar{u}_x$ at top (t), middle (m) and bottom (b) of the considered plate ($n_g = 2$)

	$a/h = 4$				$a/h = 50$			
	3*D*	$N = 1$	$N = 6$	$N = 14$	3*D*	$N = 1$	$N = 6$	$N = 14$
$\bar{u}_z$(t)	3.043	5.452	3.074	3.043	28.53	55.61	28.81	28.54
$\bar{u}_z$(m)	2.143	4.453	2.170	2.144	28.45	55.52	28.74	28.46
$\bar{u}_z$(b)	1.901	3.456	1.928	1.901	28.43	55.44	28.71	28.44
$\bar{u}_x$(t)	−1.681	−3.111	−1.694	−1.681	−1.703	−3.092	−1.714	−1.703
$\bar{u}_x$(m)	−0.6822	−1.370	−0.6841	−0.6822	−0.8081	−1.348	−0.8101	−0.8080
$\bar{u}_x$(b)	0.08240	0.3710	0.08999	0.08266	0.08528	0.3695	0.09209	0.08553

3*D* solution is reported in [16].

Table 4 Thermal load; Non-dimensional stresses $\bar{\sigma}_{ij}$ at top (t), middle (m) and bottom (b) of the considered plate ($n_g = 2$)

	$a/h = 4$				$a/h = 50$			
	3*D*	$N = 1$	$N = 6$	$N = 14$	3*D*	$N = 1$	$N = 6$	$N = 14$
$\bar{\sigma}_{xx}$(t)	−1018	−241.2	−1015	−1018	−1003	−235.7	−1001	−1003
$\bar{\sigma}_{xx}$(m)	−204.8	−989.9	−197.2	−204.7	−251.2	−980.1	−244.4	−251.2
$\bar{\sigma}_{xx}$(b)	−73.53	884.6	−108.8	−74.03	−76.10	893.1	−107.4	−76.59
$\bar{\sigma}_{xz}$(m)	4.186	3.9833	5.036	4.203	0.3122	0.3292	0.3742	0.3135
$\bar{\sigma}_{zz}$(m)	6.217	−521.8	17.10	6.300	0.04067	−469.61	9.3567	0.1178

3*D* solution is reported in [16].

it is seen that a thermal load requires higher-order thickness assumptions. As stated in the previous section, this is due to the coupling between the thermal and the mechanical field claiming higher order thickness assumptions to obtain the same accuracy.

CONCLUSIONS

In this work an extension of Unfied Formulation (UF) has been presented accounting for functionally graded plates subjected to thermal loads. It has been demonstrated that the unified treatment of all considered variables (displacements, temperature, material), inherently included in UF, provides an adequate means for taking into account any kind of material gradient. UF for functionally graded materials provides very accurate results compared to 3*D* solutions although higher order expansions in thickness direction are mandatory. It was found that the assumption of a constant transverse deflection through the thickness is not valid in the thermal case but still a justified approximation for the mechanical loading. The influence of different material gradients is more pronounced for a thermal loading. This claims also a very precise description of the thermal field contradicting any simple through-thickness assumptions for the temperature field often found in the literature.

REFERENCES

1. D. E. Burkes and J. J. Moore, Microstructure and Kinetics of a Functionally Graded $NiTiTiC_x$ Composite Produced by Combustion Synthesis, *J. Alloys Comp.*, vol. 430, pp. 274–281, 2007.
2. H. Chung and S. Das, Processing and Properties of Glass Bead Particulate-Filled Functionally Graded Nylon-11 Composites Produced by Selective Laser Sintering, *Mater. Sci. Eng. A*, vol. 437, pp. 226–234, 2006.
3. K. A. Khor, Y. W. Gu, and Z. L. Dong, Mechanical Behavior of Plasma Sprayed Functionally Graded YSZ/NiCoCrAlY Composite Coatings, *Surface and Coatings Technology*, vol. 139, pp. 200–206, 2001.
4. J. I. Kim, W.-J. Kim, D. J. Choi, J. Y. Park, and W.-S. Ryu, Design of a C/SiC Functionally Graded Coating for the Oxidation Protection of C/C Composites, *Carbon A*, vol. 43, pp. 1749–1757, 2005.
5. Y. Miyamoto, W. A. Kaysser, B. H. Rabin, A. Kawasaki, and R. G. Ford, *Functionally Graded Materials: Design, Processing and Applications*, Kluwer Academic Publishers, New York, 1999.
6. S. Suresh and A. Mortensen, *Fundamentals of Functionally Graded Materials: Processing and Thermomechanical Behaviour of Graded Metals and Metal-Ceramic Composites*, IOM Communications, Ltd, London, 1998.
7. J. Aboudi, *Mechanics of Composite Materials: A Unified Micromechanical Approach*, Elsevier, New York, 1991.
8. M.-J. Pindera, J. Aboudi, and S. M. Arnold, Limitations of the Uncoupled, RVE-based Micromechanical Approach in the Analysis of Functionally Graded Composites, *Mech. Mater.*, vol. 20, pp. 77–94, 1995.
9. J. Aboudi, M.-J. Pindera, and S. M. Arnold, Higher-Order Theory for Functionally Graded Materials, *Comp. Part B: Eng.*, vol. 30, pp. 777–832, 1999.
10. J. Aboudi, M.-J. Pindera, and S. M. Arnold, Thermoelastic Theory for the Response of Materials Functionally Graded in Two Directions with Applications to the Free-Edge Problem, *Inter. J. Solids Struct.*, vol. 33, pp. 931–966, 1996.
11. T. Reiter, G. J. Dvorak, and V. Tvergaard, Micromechanical Models for Graded Composite Materials, *J. Mech. Phy. Solids*, vol. 45, pp. 1281–1302, 1997.
12. J. R. Zuiker, Functionally Graded Materials: Choice of Micromechanics Model and Limitation in Property Variation, *Comp. Eng.*, vol. 5, pp. 807–819, 1995.
13. Z.-Q. Cheng and R. C. Batra, Three-dimensional Thermoelastic Deformations of a Functionally Graded Elliptic Plate, *Comp. Part B: Eng.*, vol. 31, pp. 97–106, 2000.
14. G. N. Praveen and J. N. Reddy, Nonlinear Transient Thermoelastic Analysis of Functionally Graded Ceramic-Metal Plates, *Inter. J. Solids Struct.*, vol. 35, pp. 4457–4476, 1998.
15. J. N. Reddy, Analysis of Functionally Graded Plates, *Inter. J. Numer. Meth. Eng.*, vol. 47, pp. 663–684, 2000.
16. J. N. Reddy and Z.-Q. Cheng, Three-dimensional Thermomechanical Deformations of Functionally Graded Rectangular Plates, *Euro. J. Mech. A Solids*, vol. 20, pp. 841–855, 2001.
17. E. Carrera, A Class of Two Dimensional Theories for Multilayered Plates Analysis, *Atti Accademia delle Scienze di Torino, Mem Sci. Fis.*, vol. 19–20, pp. 49–87, 1995.
18. E. Carrera, S. Brischetto, and A. Robaldo, *Comparison of Various Kinematics for the Analysis of Functionally Graded Materials Plates*, presented on ACME 2007, Glasgow (U.K.), 2–3 April 2007.
19. E. Carrera, S. Brischetto, and A. Robaldo, Variable Kinematic Model for the Analysis of Functionally Graded Materials Plates, *AIAA Journal*, vol. 46, no. 1, pp. 194–203, 2008.

20. S. Brischetto and E. Carrera, *Mixed Theories for the Analysis of Functionally Graded Materials plates*, presented on AIMETA 2007, Brescia (Italy), 14–17 September 2007.
21. E. Carrera and L. Demasi, Classical and Advanced Multilayered Plate Elements Based Upon PVD and RMVT. Part I. Derivation of Finite Element Matrix, *Inter. J. Numer. Meth. Eng.*, vol. 55, pp. 191–231, 2002.
22. E. Carrera and L. Demasi, Classical and Advanced Multilayered Plate Elements Based Upon PVD and RMVT. Part II. Numerical Implementations, *Inter. J. Numer. Meth. Eng.*, vol. 55, pp. 253–291, 2002.
23. T. Mori and K. Tanaka, Average Stress in Matrix and Average Elastic Energy of Materials with Misfitting Inclusions, *Acta Metal.*, vol. 21, pp. 571–574, 1973.
24. Y. Benveniste, A New Approach to the Application of Mori–Tanaka's Theory in Composite Materials, *Mech. Mater.*, vol. 6, pp. 147–157, 1987.
25. H. Hatta and M. Taya, Effective Thermal Conductivity of a Misoriented Short Fiber Composite, *J. Appl. Phy.*, vol. 58, pp. 2478–2486, 1985.
26. V. M. Levin, Thermal Expansion Coefficients of Heterogeneous Materials, *Mekh. Tverd. Tela*, vol. 2, pp. 88–94, 1967.
27. R. A. Shapery, Thermal Expansion Coefficients of Composite Materials Based on Energy Principles, *J. Comp. Mater.*, vol. 2, pp. 380–404, 1968.
28. K. Bhaskar, T. K. Varadan, and J. S. M. Ali, Thermoelastic Solution for Orthotropic and Anisotropic Composites Laminates, *Comp. Part B*, vol. 27, pp. 415–420, 1996.

APPENDIX A

If the considered plate is subjected to a bi-sinusoidal thermal load at the top and the bottom, the thermal boundary conditions are:

$$\begin{aligned} &T = 0 \quad \text{at } x = 0, a \text{ and } y = 0, b \\ &T = T_b \sin\left(\frac{m\pi x}{a}\right) \sin\left(\frac{n\pi y}{b}\right) \quad \text{at } z = -\frac{h}{2} \quad \text{with } b : \text{bottom} \\ &T = T_t \sin\left(\frac{m\pi x}{a}\right) \sin\left(\frac{n\pi y}{b}\right) \quad \text{at } z = +\frac{h}{2} \quad \text{with } t : \text{top} \end{aligned} \tag{45}$$

where m and n are the wave numbers along the two in-plane plate directions (x, y). a and b are the plate dimensions, h is the plate thickness, and T_b and T_t are the amplitudes of the temperature at the bottom and top, respectively.

In the case of multi-layered structures, continuity conditions for the temperature T and the heat flux q_z hold in the thickness direction at each kth layer interface, reading:

$$T_t^k = T_b^{k+1} \quad q_{zt}^k = q_{zb}^{k+1} \quad \text{for } k = 1, \ldots, N_l - 1 \tag{46}$$

where N_l is the number of layers in the considered structure.

The relationship between heat flux and temperature is given as:

$$q_z^k = K_3^k \frac{\partial T^k}{\partial z} \tag{47}$$

In general for the kth homogeneous orthotropic layer, the differential Fourier equation of heat conduction reads:

$$K_1^k \frac{\partial^2 T}{\partial x^2} + K_2^k \frac{\partial^2 T}{\partial y^2} + K_3^k \frac{\partial^2 T}{\partial z^2} = 0 \tag{48}$$

K_1^k, K_2^k, and K_3^k are the thermal conductivities along the three plate directions, x, y, and z, that are constant in each "classical" layer while they vary through the thickness in FGM layers. ∂ indicates the partial derivative.

For a "classical" layer, both governing equations and boundary conditions are satisfied by assuming the following temperature field:

$$T(x, y, z) = f(z) \sin\left(\frac{m\pi x}{a}\right) \sin\left(\frac{n\pi y}{b}\right) \tag{49}$$

with

$$f(z) = T_0 \exp\left(s^k z\right) \tag{50}$$

Here, T_0 is a constant and s^k a parameter. Substituting Eq. (49) in Eq. (48) and solving for s^k, we obtain:

$$s_{1,2}^k = \pm\sqrt{\frac{K_1^k(\frac{m\pi}{a})^2 + K_2^k(\frac{n\pi}{b})^2}{K_3^k}} \tag{51}$$

Therefore:

$$f(z) = T_{01}^k \exp\left(s_1^k z\right) + T_{02}^k \exp\left(s_1^k z\right) \quad \text{or} \quad f(z) = C_1^k \cosh\left(s_1^k z\right) + C_2^k \sinh\left(s_1^k z\right) \tag{52}$$

The solution for a "classical" layer k can be written as:

$$T_c(x, y, z) = T^k = \left[C_1^k \cosh\left(s_1^k z\right) + C_2^k \sinh\left(s_1^k z\right)\right] \sin\left(\frac{m\pi x}{a}\right) \sin\left(\frac{n\pi y}{b}\right) \tag{53}$$

wherein the coefficients C_1^k and C_2^k are constant for each classical layer k.

In the case of a FGM layer, the coefficients K_1^k, K_2^k, and K_3^k depend on the thickness coordinate z. Therefore, Fourier's equation does not hold in the simple form given in Eq. (48). In fact, the continuously varying thermal conductivities in a FGM layer avoid an analytical solution as shown before.

This problem can be fixed if we know the thickness law of the coefficients K_1^k, K_2^k, and K_3^k. We resolve Eq. (48) with a mathematical layer-wise method. The underlying idea is to divide the kth FGM layer in N_{ml} mathematical layers with constant properties. Then, the procedure illustrated above for the kth layer is also applied to the jth mathematical layer.

In a FGM layer the laws for the conductivity coefficients along the thickness z have the following form:

$$\left(K_1^k(z), K_2^k(z), K_3^k(z)\right) = \left(K_{10}^k, K_{20}^k, K_{30}^k\right) g(z) \tag{54}$$

where K_{10}^k, K_{20}^k, and K_{30}^k are constants and $g(z)$ is a particular function of the thickness coordinate z.

We can divide the kth FGM layer in a certain number of mathematical layers N_{ml} for which each layer j is assumed to possess constant values of the coefficients K_1, K_2, and K_3. Those constant, "effective" properties are calculated by taking the mean of the values that are obtained at the interfaces of the mathematical layers by applying Eq. (54), yielding K_1^j, K_2^j, and K_3^j for each mathematical layer j. For each mathematical layer j the parameter s_1 is given as:

$$s_1^j = \sqrt{\frac{K_1^j(\frac{m\pi}{a})^2 + K_2^j(\frac{n\pi}{b})^2}{K_3^j}} \tag{55}$$

From Eq. $(52)_2$, the amplitude of the temperature reads:

$$f(z) = C_1^j \cosh\left(s_1^j z\right) + C_2^j \sinh\left(s_1^j z\right) \tag{56}$$

In Eq. (56) for each mathematical layer j two unknowns (C_1^j and C_2^j) remain. Therefore, if the number of mathematical layers is N_{ml}, the number of unknowns is $2N_{ml}$ and we need $2N_{ml}$ equations to determine the unknowns.

As we know the temperature at the top and the bottom surface, we have already two conditions:

$$\begin{aligned} T_{top} &= C_1^1 \cosh\left(s_1^1 z_{top}\right) + C_2^1 \sinh\left(s_1^1 z_{top}\right) \\ T_{bot} &= C_1^{N_{ml}} \cosh\left(s_1^{N_{ml}} z_{bot}\right) + C_2^{N_{ml}} \sinh\left(s_1^{N_{ml}} z_{bot}\right) \end{aligned} \tag{57}$$

Another $(N_{ml} - 1)$ equations can be obtained from the continuity of temperature at each mathematical interface, and finally $(N_{ml} - 1)$ equations result from the continuity of the heat flux through the mathematical interfaces, compare Eq. (46). Thus, we have:

$$\begin{aligned} &C_1^j \cosh\left(s_1^j z_t^j\right) + C_2^j \sinh\left(s_1^j z_t^j\right) - C_1^{j+1} \cosh\left(s_1^{j+1} z_b^{j+1}\right) + C_2^{j+1} \sinh\left(s_1^{j+1} z_b^{j+1}\right) = 0 \\ &s_1^j K_3^j \left[C_1^j \cosh(s_1^j z_t^j) + C_2^j \sinh(s_1^j z_t^j)\right] \\ &- s_1^{j+1} K_3^{j+1} \left[C_1^{j+1} \cosh\left(s_1^{j+1} z_b^{j+1}\right) + C_2^{j+1} \sinh\left(s_1^{j+1} z_b^{j+1}\right)\right] = 0 \end{aligned} \tag{58}$$

In Eqs. (57) and (58), z_{top} and z_{bot} indicate the coordinates of top and bottom of the whole FGM layer. z_t^j and z_b^{j+1} represent the top of the jth mathematical layer and the bottom of the $(j+1)$th mathematical layer, respectively.

Resolving the system given by Eqs. (57) and (58), we gain the $2N_{ml}$ coefficients C_1^j and C_2^j. The actual temperature in the kth FGM layer is then given by:

$$T_c(x, y, z) = T^j = \left[C_1^j \cosh\left(s_1^j z\right) + C_2^j \sinh\left(s_1^j z\right)\right] \sin\left(\frac{m\pi x}{a}\right) \sin\left(\frac{n\pi y}{b}\right) \tag{59}$$

We compute the temperature at different values z_N of the thickness coordinate. By solving the system Eq. (60), we obtain the N values of θ_τ for the Unified

Formulation:

$$\begin{bmatrix} T_c(z_1) \\ T_c(z_2) \\ \vdots \\ T_c(z_N) \end{bmatrix} = \begin{bmatrix} F_0(z_1) & F_1(z_1) & \cdots & F_N(z_1) \\ F_0(z_2) & F_1(z_2) & \cdots & F_N(z_2) \\ \vdots & \vdots & \vdots & \vdots \\ F_0(z_N) & F_1(z_N) & \cdots & F_N(z_N) \end{bmatrix} \begin{bmatrix} \theta_0 \\ \theta_1 \\ \vdots \\ \vdots \\ \theta_N \end{bmatrix} \tag{60}$$

So, if we consider a generic kth FGM layer, the temperature profile is approximated by Eq. (6) and the N values of θ_τ^k are given by Eq. (60).

APPENDIX B

The explicit expressions of the fundamental nuclei are listed below for the case of a closed form solution. $\alpha = m\pi/a$ and $\beta = n\pi/b$, with m and n as the wave numbers in in-plane directions and a and b as the plate dimensions.

- $K_{u\theta}$

$$\begin{aligned} K_{u\theta_{11}} &= -\alpha E_{\tau sr}(\lambda_{pp1r} + \lambda_{pn1r}) \\ K_{u\theta_{12}} &= K_{u\theta_{13}} = K_{u\theta_{21}} = 0 \\ K_{u\theta_{22}} &= -\beta E_{\tau sr}(\lambda_{pp2r} + \lambda_{pn2r}) \\ K_{u\theta_{23}} &= K_{u\theta_{31}} = K_{u\theta_{32}} = 0 \\ K_{u\theta_{33}} &= E_{\tau sr}(\lambda_{nn3r} + \lambda_{np3r}) \end{aligned}$$

- K_{uu}

$$\begin{aligned} K_{uu_{11}} &= C_{55r}E_{\tau_{,z}s_{,z}r} + C_{11r}\alpha^2 E_{\tau sr} + C_{66r}\beta^2 E_{\tau sr} \\ K_{uu_{12}} &= C_{12r}\alpha\beta E_{\tau sr} + C_{66r}\alpha\beta E_{\tau sr} \\ K_{uu_{13}} &= -C_{13r}\alpha E_{\tau_{,z}sr} + C_{55r}\alpha E_{\tau s_{,z}r} \\ K_{uu_{21}} &= K_{uu_{12}} \\ K_{uu_{22}} &= C_{44r}E_{\tau_{,z}s_{,z}r} + C_{22r}\beta^2 E_{\tau sr} + C_{66r}\alpha^2 E_{\tau sr} \\ K_{uu_{23}} &= -C_{23r}\beta E_{\tau_{,z}sr} + C_{44r}\beta E_{\tau s_{,z}r} \\ K_{uu_{31}} &= C_{55r}\alpha E_{\tau_{,z}sr} - C_{13r}\alpha E_{\tau s_{,z}r} \\ K_{uu_{32}} &= C_{44r}\beta E_{\tau_{,z}sr} - C_{23r}\beta E_{\tau s_{,z}r} \\ K_{uu_{33}} &= C_{33r}E_{\tau_{,z}s_{,z}r} + C_{44r}\beta^2 E_{\tau sr} + C_{55r}\alpha^2 E_{\tau sr} \end{aligned}$$